Harla Journals

Harla Journal of Applied Science and Materials
Journal home page:
https://journals.ddu.edu.et/index.php/HJASM

Harla journal
of Applied Science and Materials

The effect of Tb/Yb co-doping on the optical, morphology, and structural properties of $YV_{0.5}P_{0.5}O_4$

Molebatsi D[1], Mokoena M[3,4], A.U Yimamu[2*], Motloung S.J.[1] and Tshabalala K.G.[1]

[1]Department of Physics, University of the Free State (QwaQwa Campus), Private Bag X 13, Phuthaditjhaba, 9866, South Africa
[2]Department of Physics, College of Natural Sciences, Dire Dawa University, Dire Dawa, Ethiopia.
[3]Biomedical Engineering Research Centre, Department of Human Biology, University of Cape Town, Private Bag X 3, Anzio Road, 7077, South Africa
[4]National Laser Centre, Council for Scientific and Industrial Research, P.O. Box 395, Pretoria 0001, South Africa
**Corresponding Author*

Abstract

Terbium-ytterbium-doped yttrium orthophosphovanadate powders were synthesized using the chemical bath deposition (CBD) method at a constant temperature of 80 °C. The effect of Tb/Yb co-doping on the optical, morphological, and structural properties of $YV_{0.5}P_{0.5}O_4$ was investigated. X-ray diffraction (XRD) analysis confirmed the structure of $YV_{0.5}P_{0.5}O_4$:1mol%Tb*x*%Yb as tetragonal. Furthermore, the incorporation of the dopants did not alter the structure of the pristine material, however, a reduction in the crystallite size was observed. Scanning electron microscopy (SEM) images revealed that the synthesized nano powder consisted of agglomerated primary spherical nanorods, oval particles, and secondary tetragonal-like structures. The chemical elements present in the intended compound were verified by energy-dispersive X-ray spectroscopy (EDS) which were Y (yttrium), V(vanadium), O (oxygen), P (phosphorus), Tb (terbium), and Yb (ytterbium). Fourier transform infrared spectroscopy (FTIR) revealed that the sample consisted of functional groups of O-H, N-O, V-O, P-O, and H-O-H. Ultraviolet-visible (UV-Vis) spectroscopy displayed absorption band at 981 nm associated with f→f transitions of the dopants. Additionally, a strong absorption band between 250 nm and 300 nm, is related to the absorption by the hosts species VO_4^{3-} and PO_4^{3-}.

Key words/Phrases: orthophosphovanadate; optical; morphology; and nanopowder

1. Introduction

High purity, single phase, and uniform particle size optical materials are very crucial for the development of photonic devices due to their high resolution and high luminescence efficiency [1], with enhancement properties from rare earths. Rare earth metals have attracted the attention of many researchers due to their properties. Rare earth metals, which include about 17% of all naturally occurring elements, are a group of 17 chemically comparable elements [2]. These include the fifteen lanthanides on the periodic table as well as scandium and yttrium. The wide application of lanthanum compounds is based on the fact that lanthanides, with their specific 4f electron configuration, have different coordination numbers from 6 up to 12, screened by the filled $5p^6 6s^2$ orbitals [2 –4].

**Corresponding author: A.U Yimamu; email: ahemed.dilla2010@gmail.com; Cell phone: +251930509797*

Received: March 2024; Received in revised form: May 2024; Accepted: June 2024

Lanthanide ions exhibit very low molar absorption coefficients, narrow-line emission, mostly in the visible and near infrared region, and long excited state lifetimes [4, 5]. Therefore, nanoparticles doped with trivalent lanthanide (Ln^{3+}) ions have gained interest due to their potential applications in three-dimensional displays, optical sensors, solid-state lasers and solar cells and have been extensively studied [6]. With the development of nanotechnology, Ln^{3+} ion-doped nanoparticles with various color emissions have been successfully synthesized [7, 8].

In this study, we focus on the co-doping of earth orthovanadate and earth phosphates, specifically orthophosphates. The stoichiometric representation for rare earth orthovanadate and lanthanide phosphates are as follows: $LnVO_4$ (Ln = rare earth ion) and $LnPO_4$ [9, 10]. Lanthanide-doped yttrium orthophosphate (YPO_4: Ln^{3+}) has proven to be an ideal candidate for optoelectronic components due to its high thermal stability, quantum efficiency, and refractive index [11 – 14]. Among various Ln^{3+}-doped luminescent nanomaterials, up-converting rare earth orthophosphates such as $LaPO_4$ and YPO_4 doped with Yb^{3+} ions show superior physicochemical properties. They are resistant to photodegradation, oxidation, and high temperature (HT) [15]**.** Furthermore, such materials are insoluble in water (forming stable aqueous colloids), and their synthesis is simple, reproducible, and inexpensive [16, 17]. Yb^{3+} ions act as proficient sensitizers due to their high absorption cross-section in the mentioned NIR range [18]. Among the lanthanide ions, europium (III) ions and terbium (III) ions were most frequently used as sensitizers due to their specific spectroscopic properties [18]. However, the focus of this study is on terbium (III) ions. It has sufficiently large energy gap between the excited and the ground state of $\Delta E \sim 14{,}800$ eV ($^5D_4 \rightarrow {}^7F_0$), it shows large differences between the emission and excitation wavelengths (high Stokes shift), which minimizes the overlapping of excitation and emission spectra (λ_{ex} = 368 nm, $\lambda_{em} \sim$ 490 nm), 545 nm for Tb (III) ions, it has long- lived excited states and energies of these ions are lower ($^5D_0 \sim 17{,}267$ cm^{-1} and $^5D_4 \sim 20{,}500$ cm^{-1}) than the triplet states energies of many organic compounds [19]**.**

On the other hand, yttrium orthovanadates have proved to be one of the best hosts for luminescent materials with a very high energy transfer (ET) efficiency for the VO_4^{3-} group [20]. Various studies have been carried out on YVO_4 and YPO_4 as single compounds and doped; it is of interest to study the behaviour of the two compounds combined and co-doped.

The two compounds can be combined by substituting P^{5+} with V^{5+} relatively. The crystal structures of the YPO_4 host matrix differ depending on the selected synthesis method, namely monoclinic, tetragonal, and hexagonal, which are referred to as churchite structures, xenotime structures, and rhabdophane structures [21]. Recently, some researchers reported that YPO_4 phosphor synthesized by the wet chemical route method crystallizes in a hydrated hexagonal state [22]. According to the current literature, the luminescence properties can be effectively controlled by regulating the structure phase [22]. Therefore, nanoparticles are specifically designed by using the synthesis conditions to control the crystalline structure [22]. Therefore, it is very important to consider the nature of the synthetic method concerning the kind of structure to be achieved. This leads to the choice of synthesis method used in this study, namely chemical bath deposition. Chemical bath deposition has low process temperature, scalability, and reproducibility, low cost for large-scale production, high efficiency, and is simple [23]. Therefore, the optical, morphological, and structural properties of rare earth co-doped orthophosphovanadate powderspreparedby using the mentioned synthesis method were investigated.

2. Experimental

2.1. Synthesis

Ammonium metavanadate (NH_4VO_3) (purity = 99%), ammonium dihydrogen phosphate ($NH_4H_2PO_4$), Yttrium (III) nitrate hexahydrate ($Y(NO_3)_3.6(H_2O)$) (99.8% trace metal basis), ammonia (25% NH_3), Ytterbium (III) acetate hydrate ($C_6H_9O_6Yb.xH_2O$ 99.5% trace metal basis) and Terbium (III) nitrate pentahydrate ($N_3O_9Tb.5H_2O$ 99,9%) were used. The chemicals used were of analytical-grade reagents and no further purification was required before use. Deionized water was also used for the preparation of nanopowders. During the preparation, NH_4VO_3 was dissolved in 50 mL of deionized water and stirred with a magnetic stirrer on a hot plate. Heat was used since metavanadate takes a long time to dissolve. $NH_4H_2PO_4$ was dissolved in another 50 mL of deionized water. $(YNO_3)_3.6(H_2O)$, 1 mol% $N_3O_9Tb.5H_2O$ and $C_6H_9O_6Yb.xH_2O$ (x = 1, 3, 5, 7, and 10 mol%) were dissolved in a beaker containing 50 mL of deionized water. NH_4OH solution was poured into a burette and used as a precipitant. A round bottom centrifuge tube was placed in a water bath that was maintained at 80°C, 50 mL of $(YNO_3)_3.6(H_2O)$), 1 mol% $N_3O_9Tb.5H_2O$ and $C_6H_9O_6Yb.xH_2O$ (1 mol%, 3 mol%, 5 mol%, 7 mol%, 10 mol%) solution, 50 mL of $NH_4H_2PO_4$ solution and 50 mL of NH_4VO_3 solution were added to a round bottom centrifuge tube with vigorous stirring. A pale-yellow precipitate was formed. Then 50 mL of NH_4OH was added dropwise into the pale-yellow precipitate, and the colour changed to white. The amalgam was allowed to cool at room temperature. Then the precipitate was filtered using suction filtration equipment, followed by washing with 50 mL of ethanol and deionized water to remove impurities. The collected precipitates were allowed to dry for 72 hours. Finally, $YV_{0.5}P_{0.5}O_4$:1mol%TbxYb (x = 1, 3, 5, 7, 10 mol%) were grinded, and the nanopowders were ready for characterization.

2.2. Characterization

The $YV_{0.5}P_{0.5}O_4$:1%TbxYb (x = 1, 3, 5, 7, 10 mol%) nanopowders were analyzed using different techniques. XRD was used to determine crystallinity, structure, and crystallite size. The 2θ measurements were carried out with radiation of CuKα (1.5418Å) from 20° to 60°. SEM which uses a beam of high- energy electrons in a raster-scan pattern [24], measured orientation and morphology of the specimen with Tescan Vega 3 equipped with Oxford X-Max. EDS provided more important data and images regarding qualitative and quantitative information [25] of the microstructure of the nanopowders. FTIR spectroscopy was performed to obtain the absorption and functional groups of nanopowders in the infrared range from 650 to 4000 cm^{-1} using PerkinElmer. UV-Vis was performed to determine the diffuse reflectance measurements and estimate the bandgaps of the samples using PerkinElmer UV WinLab 6.2.0.0741 at the Lamda of 900.

3 Results and discussion

3.1. Structural analysis

The crystallinity the structure of $YV_{0.5}P_{0.5}O_4$:1%TbxYb where x = 1, 3, 5, 7, and 10 mol% were studied using XRD. Figure 1 shows the XRD spectra of $YV_{0.5}P_{0.5}O_4$:1%TbxYb along with the corresponding JCPDS files. $YV_{0.5}P_{0.5}O_4$:1mol%TbxYb has a crystallite size ranging from 20.02 nm to
5.337 nm and lattice parameters of $a = b$ = 3.648 Å and c = 3.6099 Å. The reflection planes of (200) and (004), corresponding to 2θ of 25,01° and 56,69 ° were used respectively. The Debye-Scherrer (equation 1) was then used to estimate the crystallite size [26]

$$D = \frac{k\lambda}{\beta\cos\theta} \quad (1)$$

where D is the crystallite size, $k = 0.9,$, β is the full-width half maximum (FWHM) and θ is the Bragg diffraction angle. The lattice parameters of a tetragonal structure were calculated using

$$\frac{1}{d^2} = \frac{h^2+k^2}{a^2} + \frac{l^2}{c^2} \quad (2)$$

where (hkl) are the Miller indices, d is the d-spacing from the Bragg equation [27]

$$n\lambda = 2d\sin\theta \quad (3)$$

additionally, the Williamson-Hall formula [28]

$$\beta\cos\theta = \frac{k\lambda}{D} + 4\varepsilon\sin\theta \quad (4)$$

was used to confirm the particle size obtained using equations (1). All samples show a combination of the diffraction pattern of the standard tetragonal structures of YPO_4 and YVO_4 corresponding to the JCPDS file numbers 11-0254 and 17-0341 respectively. The spectra show a slight shift towards lower angles compared to the spectrum of pure YPO_4 and a very slight shift towards higher angles compared to the pure YVO_4 spectrum, this is because the two compounds have been combined, and due to the difference in the ionic radii of the V (0.35Å) and P (0.17Å) which induces strain [29]. The resulting $YV_{0.5}P_{0.5}O_4$:1%TbxYb peaks therefore lie between the YPO_4 and YVO_4 peaks, the results obtained were intentional and therefore expected. The W-H method represented in Figure 2 was used to estimate the strain (C) which ranged from 0.00888 to 0.0218. The addition of the dopants affected the intensity of the peaks. The peak intensities of $YV_{0.5}P_{0.5}O_4$:1%TbxYb (x = 1 mol%) is greater compared to the other doped samples (x =3, 5, 7, and 10 mol%) respectively. Excessive doping disrupted the crystallinity of the samples and induced strain, hence the intensity reduced as the doping concentration was increased. The peaks of $YV_{0.5}P_{0.5}O_4$:1%TbxYb (x = 1 mol%) are sharper compared to the peaks of the (x =3-10 mol%) samples, which implies that the crystallite size is larger compared to the other samples, and the crystallinity is compromised as more Yb dopant is added to the host.

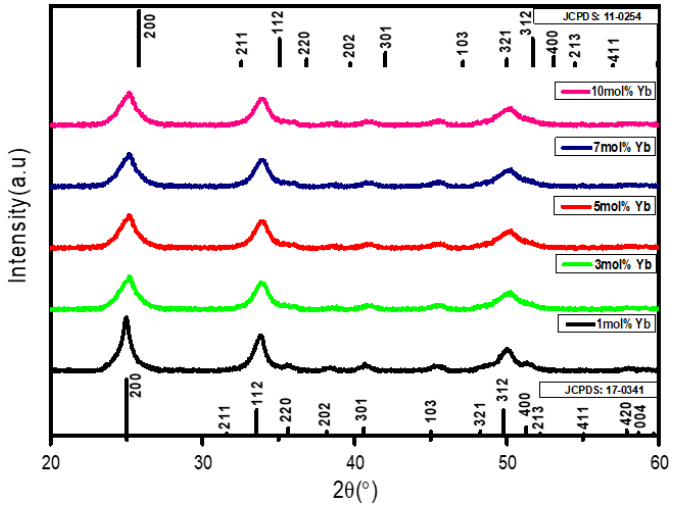

Figure 1. XRD pattern for $YV_{0.5}P_{0.5}O_4$:1%TbxYb (x = 1, 3, 5, 7, and 10 mol%), JCPDS:11-0254 corresponds to YPO_4 and JCPDS:17-0341 corresponds to YVO_4.

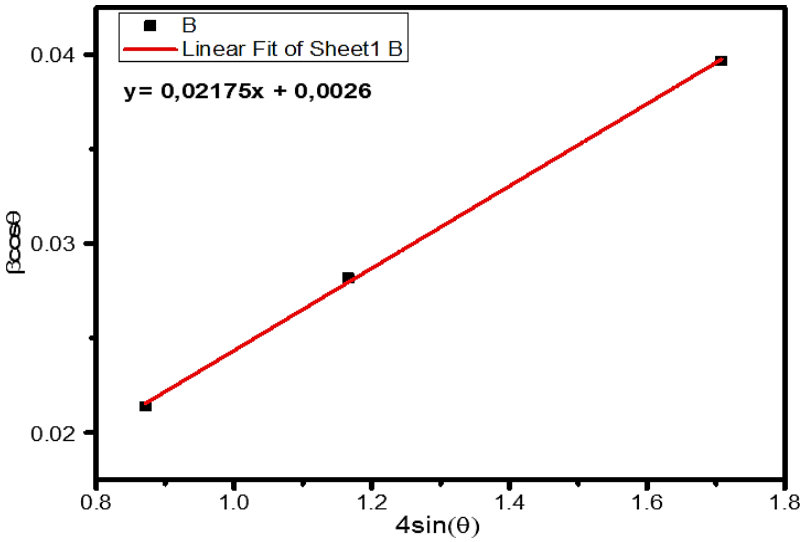

Figure 2. Linear plot of $YV_{0.5}P_{0.5}O_4$:1mol%Tb10mol%Yb for strain and crystallite size.

3.2. Morphology analysis

Figure 3 shows the SEM images of $YV_{0.5}P_{0.5}O_4$:1%Tb1*x*Yb nanopowders. These images show that the powder mainly comprises of agglomerated spherical particles. The size of the agglomerates is small and irregular. The particles appear to be randomly oriented. At high magnification, very few rods and oval shapes are visible from the images. At low and high magnification (images c and f), the secondary particles are formed from primary particles (smaller particles). The more dopant is incorporated, the better the formation of the secondary particles, which resemble the tetragonal structure, especially in Figure 3(c). This is in relation to the XRD results obtained for the structure type obtained in this study.

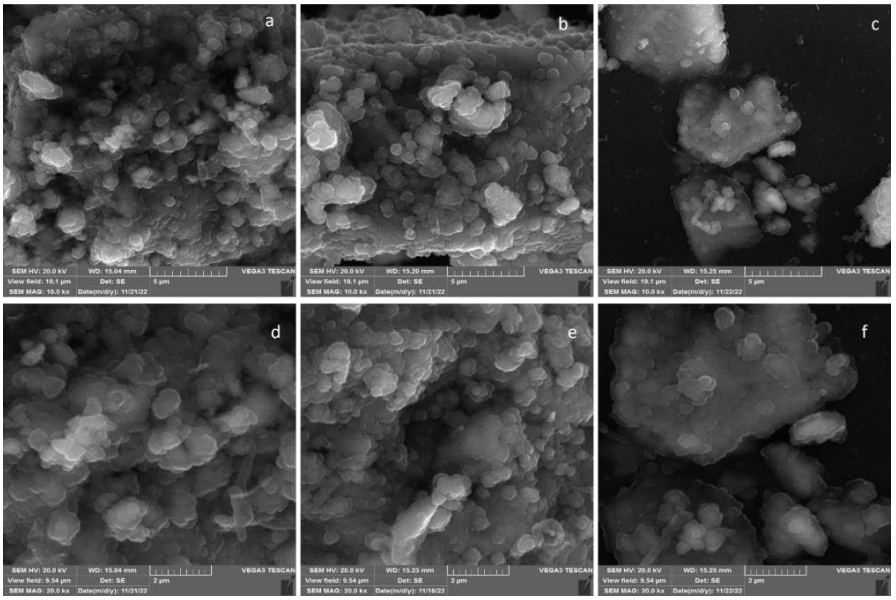

Figure 3. SEM images of $YV_{0.5}P_{0.5}O_4$:1%Tb*x*Yb nanopowders at low magnification (a, b, and c) and high magnification (d, e, and f).

3.3. Elemental analysis

Figure 4 shows the EDS spectrum of $YV_{0.5}P_{0.5}O_4$:1%Tb1mol%Yb nanopowder. The EDS validates the presence of V, O, Tb, P, Y, V, Yb, and carbon (C) which was used to coat the sample during the measurements. The table insert on the spectrum gives the weight percent of all the elements picked up by the EDS. The weight concentration of yttrium exceeds the concentration of all other elements, and the lowest weight concentration has been recorded from Tb and Yb dopants because of their relatively low concentration. The EDS spectrum and the corresponding elemental mapping confirm the formation of $YV_{0.5}P_{0.5}O_4$:1%Tb1mol%Yb nanopowder and the homogeneous distribution of the elements present on the surface of the sample (Figure 5).

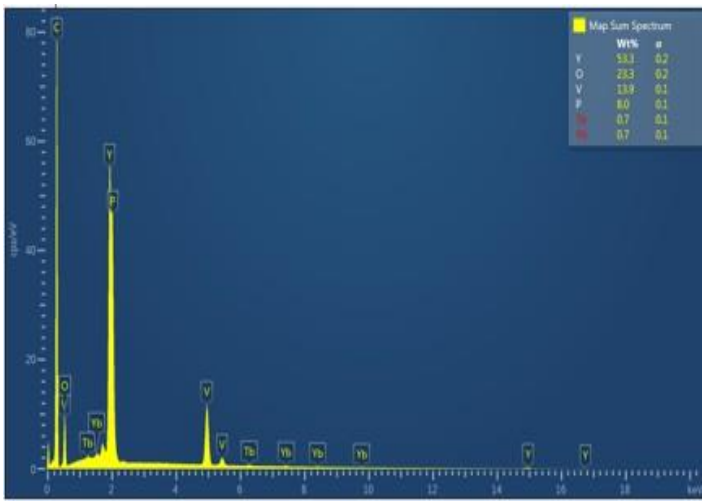

Figure 4. EDS spectrum for $YV_{0.5}P_{0.5}O_4$:1mol%Tb1mol%Yb

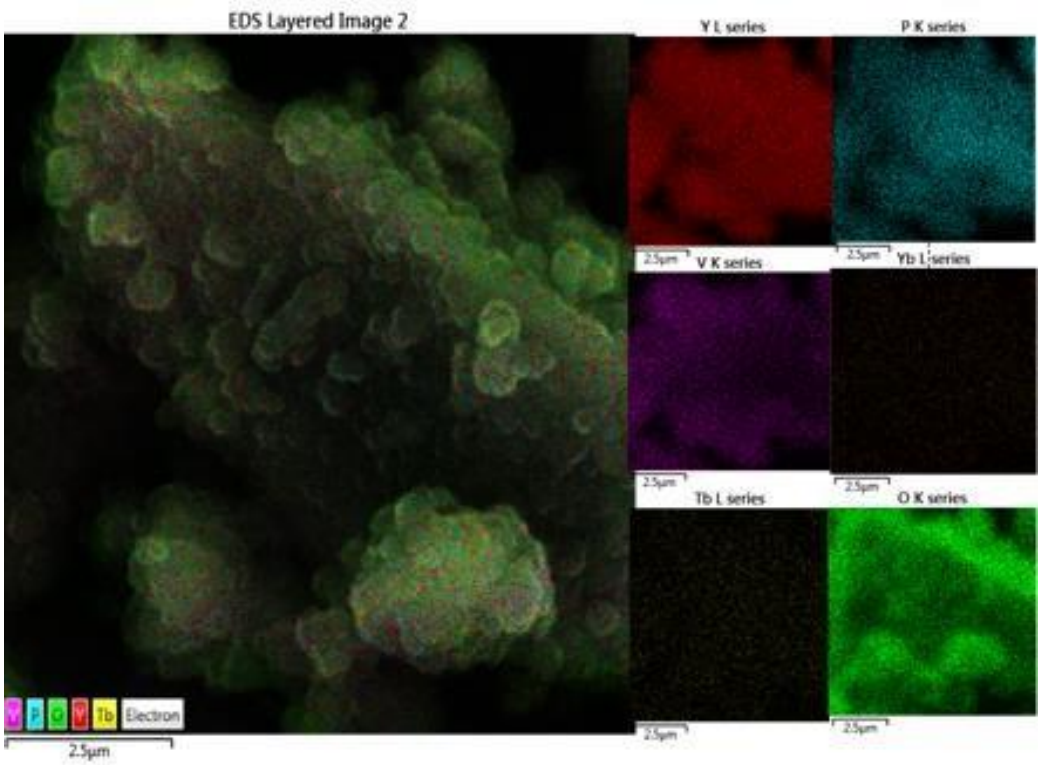

Figure 5. EDS elemental mapping $YV_{0.5}P_{0.5}O_4$:1mol%Tb1mol%Yb

3.4. Chemical bonding analysis

Figure 6 has two regions, namely the fingerprint region (1500 to 650 cm^{-1}) towards the right end of the graph, which is unique to the samples prepared and on the left region is the functional group region, also known as the diagnostic region [30, 31]. The functional group region has various prominent points which we call peaks. The spectra show a series of absorptions peaks from 665 to 3683 cm^{-1}. A broad absorption peak around 3242 cm^{-1} corresponds to the OH group [32] which correlates with the deionized water used during sample preparation. The peaks at 807 cm^{-1}, 1002 cm^{-1}, 1053 cm^{-1}, 1380 cm^{-1}, and 1624 cm^{-1} correlate with V-O, P-O, P-O, N-O, and H-O-H groups, respectively. VO_4^{3-} corresponds to the apparent vibrational mode for the V-O bond [33]. PO_4^{3-} corresponds to the antisymmetric stretching vibration mode of P-O bonds [34, 35]. The N-O group corresponds to the NO_2 symmetric stretching vibration [36]. The presence of dopants showed no peaks, consistent with the XRD results, showing that the structure of the compound was not affected by the addition of dopants.

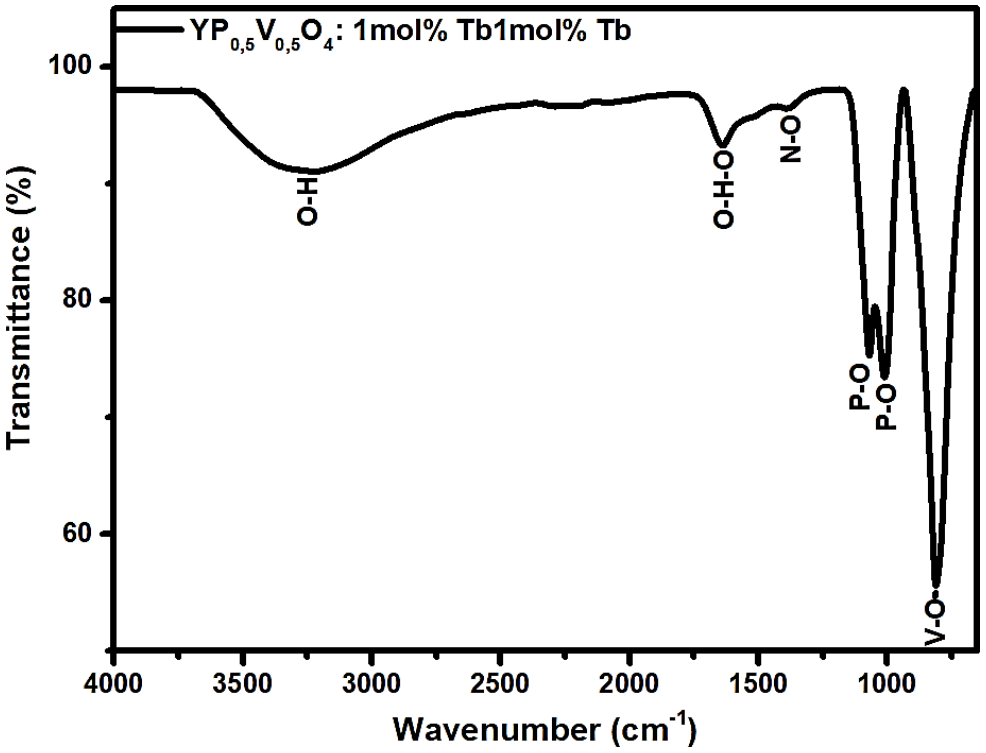

Figure 6: FTIR spectrum of $YV_{0.5}P_{0.5}O_4$:1mol%Tb1mol%Yb nanopowder.

3.5. Diffuse reflectance measurements analysis

Figure 7 shows the diffuse reflectance spectrum of $YV_{0.5}P_{0.5}O_4$:1mol%TbxYb (x = 1, 3, 5 and 10 mol%). The % reflectance on the vertical axis indicates how strongly light was reflected at each wavelength [36]. A lower % reflectance indicates that the energy is being absorbed by the amalgam. The spectra show low reflectivity at lower wavelengths between 250 nm and 300 nm range for all the samples, suggesting that there is strong absorption by the host VO_4^{3-} [37] in the UV region. The maximum reflectance is observed at a wavelength of 500 nm. The decrease in reflectivity detected at longer wavelengths indicates the f→f transition of Tb^{3+} at the wavelength of 981 nm [38]. Thus, the absorption by the dopants occurs at a wavelength of 981 nm. Bandgap estimation was obtained by using the Schuster-Kubelka-Munk [39]

$$F(R\infty) = [(1-R\infty)]^2/2R\infty = K/S \quad (5)$$

The Tauc relation is used to estimate the bandgap (E_g) where α is the linear absorption coefficient of the sample [39]

$$(\alpha hv)^2 = CI(hv - E_g)^2 \quad (6)$$

The absorption coefficient *K* is exactly 2α when the sample scatters this leads to the final equation [39]

$$((R\infty) - hv)^2 = C2(hv - E_g)^n \quad (7)$$

Figure 8 shows that the extrapolated graph exhibit a direct bandgap energy of 3.8 eV [40]. The bandgap energies of samples 1mol%Tb1mol%Yb to 1mol%Tb10mol%Yb range from 3.7 to 3.8 eV, respectively. The band gaps obtained differ from the band gap of $YV_{0.5}P_{0.5}O_4$ from the literature [41], which is due to the addition of dopants. As the molar percentage concentration of the dopants increases, the bandgap energy decreases.

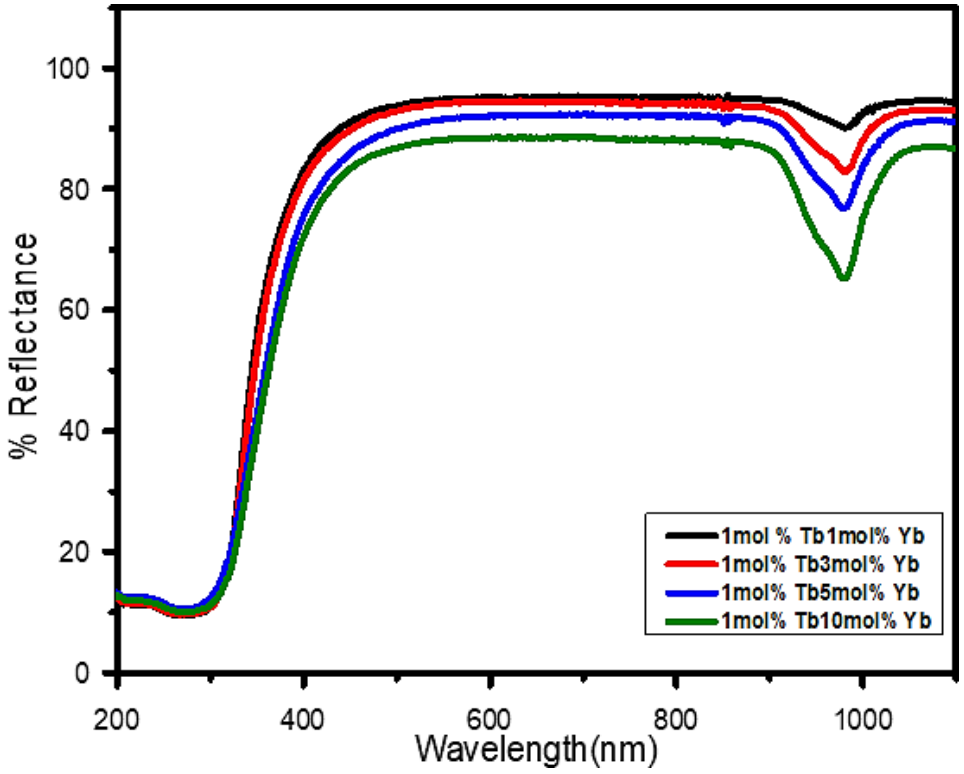

Figure 7. Diffuse reflectance measurement graphs for $YV_{0.5}P_{0.5}O_4$:1mol%Tb*x*Yb (*x* = 1, 3, 5, and 10 mol%)

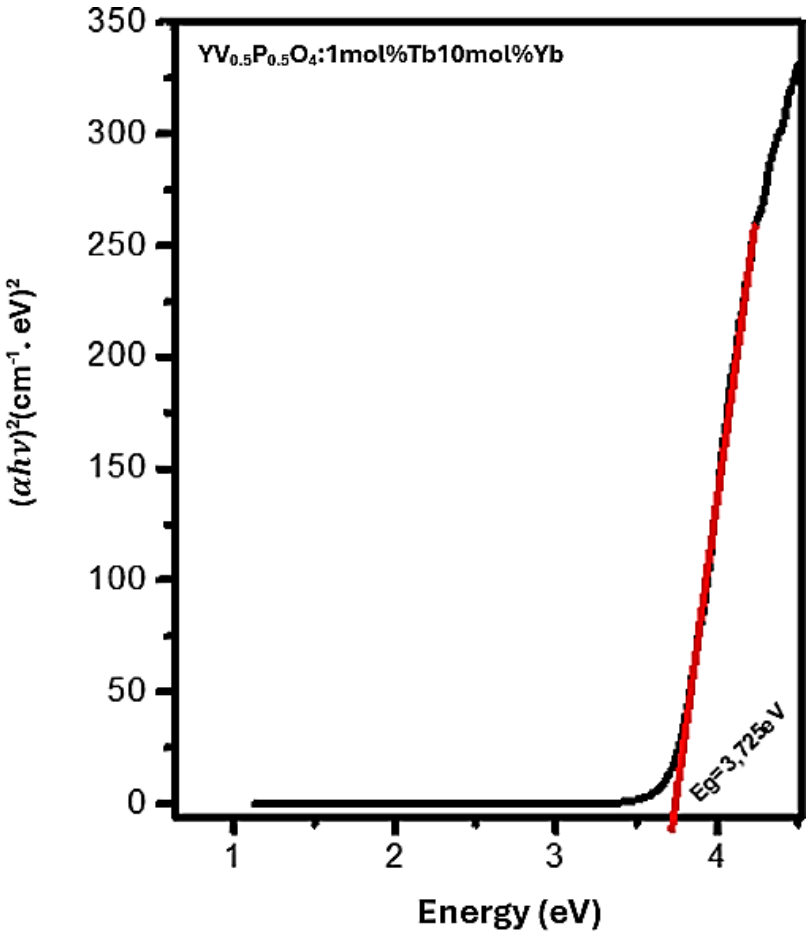

Figure 8. Tauc relation showing the bandgap energy for 1mol%Tb10mol%YbTauc relation showing direct bandgap.

Table 1: Standard and prepared sample bandgap energies for orthophosphovanadates.

Samples ID	**Bandgap energy (eV)**
YVO_4	2.750[42]
$YV_{0.5}P_{0.5}O_4$	2.830[42]
YPO_4	5.830[42]
$YV_{0.5}P_{0.5}O_4$:1mol%Tb10mol%Yb	3.725
$YV_{0.5}P_{0.5}O_4$:1mol%Tb5mol%Yb	3.773
$YV_{0.5}P_{0.5}O_4$:1mol%Tb3mol%Yb	3.783
$YV_{0.5}P_{0.5}O_4$:1mol%Tb1mol%Yb	3.795

4. Conclusion

$YV_{0.5}P_{0.5}O_4$:1mol%TbxYb was synthesized using a chemical bath deposition method. XRD data showed that the synthesized powder has a tetragonal structure that is not affected by variation in the molar percentage concentration of the dopants (Tb/Yb). In addition, it also showed that the particle size of

$YV_{0.5}P_{0.5}O_4$:1mol%Tb*x*Yb decreases as the concentration of the dopants is increased. SEM showed that the morphology of the prepared samples consisted of spheres, rods, and tetragonal-like particles. Additionally, the change in concentration of Yb did not alter the morphology of the samples. The elemental composition of the samples prepared was therefore confirmed by EDS. The functional groups identified by the FTIR in the samples were V-O, P-O, N-O, O-H-O. UV-Vis spectroscopy showed that there were transitions associated with f→f transitions of Tb^{3+} at 981 nm and strong absorption related to the absorption by the host VO_4^{3-} from 250 to 300 nm.

Acknowledgment

I would like to thank the University of the Free State for their financial support, as well as the Department of Physics for granting me access to their lab and materials for conducting research.

References

[1] S. Wang, P. Wang, Y. Ruan, Y. Wang, and S. Zhang, *Sci. Eng. Compos. Mater* **28** (2021) 205

[2] Y. Ji *et al. fchem* **7** (2019) 1

[3] K. Staszak, K. Wieszczycka, V. Marturano, and B. Tylkowski *Coord. Chem. Rev* **397** (2019) 76

[4] A. Tymiński, and Grzyb *J. Lumin*. **181** (2021) 411

[5] M. Matsuoka *et al.*, Chem Mater **17 (**2005) 1783

[6] V. Singh, A. R. Kadam, and S. J. Dhoble, *Optik (Stuttg)* **243** (2021) 167437

[7] K. Li, T. Chen, H. Mao, Y. Chen, and J. Wang, *J Electron Mater* **50** (2021) 1189

[8] S. J. Motloung, "Investigation of photoluminescent properties of rare earth doped mixed multicomponent structures of phosphovanadates", PhD Thesis, University of the Free State, Qwaqwa, South Africa, 2017

[9] T. Kegl, A. Košak, A. Lobnik, Z. Novak, A. K. Kralj, and I. Ban *J Hazard Mater* **386** (2020) 1

[10] B. Shao *et al. Inorg Chem*. **56** (2017) 6114

[11] H. Xiong *et al J Alloys Compd* **782** 2019 845

[12] B. Shao *et al. Inorg Chem* **56** 2017 6114

[13] T. Lyu and P. Dorenbos *J Mater Chem C Mater*. **6** (2018) 369

[14] T. Yuan, X. Wang, P. Li, B. Quan, and Y. Liu, *J Lumin* **201** 2018 350

[15] M. Runowski, A. Shyichuk, A. Tymiński, T. Grzyb, V. Lavín, and S. Lis, *ACS Appl Mater Interfaces* **10** (2018) 17269

[16] A. Tymiński; Grzyb, T. *J. Lumin*. **181** (2017) 411

[17] M. Matsuoka *et al. J Lumin*. **251** (2022) 119208

[18] M. Kaczmarek *J Lumin*. **222** (2020) 117174

[19] H. Xiong *et al. J Alloys Compd*. **782** (2019). 845

[20] M. Runowski, A. Shyichuk, A. Tymiński, T. Grzyb, V. Lavín, and S. Lis, *ACS Appl Mater Interfaces* **10** (2018) 17269

[21] V. Singh, A. R. Kadam, and S. J. Dhoble, *Optik (Stuttg)* **243** (2021) 167437

[22] A. Ashok, G. Regmi, A. Romero-Núñez, M. Solis-López, S. Velumani, and H. Castaneda, *J. Mater. Sci.: Mater. Electron*. **31** (2020). 7499

[23] H. Vahidi *et al. Crystals* **11** (2021) 878

[24] J. Rydz, A. Šišková, and A. Andicsová Eckstein *Advances in Materials Science and Engineering*, vol. **2019 (2019)** 6871785

[25] V. Singh, P. Kumari, S. J. Dhoble, P. Holi, H. Jeong, and V. Koteswararao, *Optik (Stuttg)* **242** (2021) 167223

[26] https://pubs.acs.org/sharingguidelines Accessed: 2024.12.02

[27] D. Nath, F. Singh, and R. Das, *Mater Chem Phys*, vol. **239** (2020) 122021.

[28] C. Marcus, J Kevin, B Derek, M Lin, M Pourkashanian, *Inorg. Chem.* **56** 2017

[29] S. J. Motloung, P. Kumari, L. F. Koao, T. E. Motaung, T. T. Hlatshwayo, and M. J. Mochane, *Mater Today Commun*, **14** (2018) 294

[30] https://chem.libretexts.org › Organic_Chemistry_I_(Liu) Accessed: 2024.12.02

[31] https://pubs.acs.org/sharingguidelines Accessed: 2024.12.02

[32] A. Dwivedi, E. Rai, D. Kumar, and S. B. Rai, *ACS Omega*. **4** (2019) 6903

[33] J. Wu *et al. J Lumin*. **245** (2022) 118791.

[34] Z. wei Zhang *et al. J Alloys Compd*. **695** (2017) 3220

[35] G. Lan *et al. Fuel*. **295** (2021) 1

[36] Available: https://chem.libretexts.org › Organic_Chemistry_I_(Liu) Accessed: 2024.12.02

[37] A. Dwivedi, E. Rai, D. Kumar, and S. B. Rai, *ACS Omega* **4** (2019) 6903

[38] K. Li, T. Chen, H. Mao, Y. Chen, and J. Wang, *J Electron Mater*. **50** (2021) 1189

[39] V. Singh, P. Kumari, S. J. Dhoble, P. Holi, H. Jeong, and V. Koteswararao, *Optik (Stuttg).* **242** (2021) 167223.

[40] B. Yang *et al. J Am Chem Soc.* **140** (2018) 17001

[41] Q. Ma, Q. Zhang, M. Yang, B. Shao, R. Ouyang, and N. Guo, *Inorg Chem*. **61** (2022) 9823